

## Using gamma-ray Spectrometry and Geostatistics for Assessing Geochemical Behaviour of Radioactive Elements in the Lese Catchment (southern Italy)

Guagliardi, I.<sup>1</sup>, Buttafuoco, G.<sup>1\*</sup>, Apollaro, C.<sup>2</sup>, Bloise, A.<sup>2</sup>, De Rosa, R.<sup>2</sup> and Cicchella, D.<sup>3</sup>

<sup>1</sup>National Research Council of Italy - Institute for Agricultural and Forest Systems in the Mediterranean (ISAFOM), Via Cavour 4/6 - 87036 Rende (CS), Italy

<sup>2</sup>Department of Earth Sciences, University of Calabria, Ponte Bucci, 87036 Rende (CS), Italy

<sup>3</sup>Department of Geological and Environmental Studies, University of Sannio, Via dei Mulini, 59/A - 82100 Benevento, Italy

Received 10 Aug. 2012;

Revised 10 March 2013;

Accepted 20 March 2013

**ABSTRACT:** Gamma-rays emitted from the ground surface relate to the primary mineralogy and geochemistry of the bedrock, and the secondary weathered materials. This information can contribute significantly to an understanding of the geochemical and pedogenetic history of a region. The main aim of this paper was to study the relationship between ground gamma-ray data and basement geochemistry in the Lese catchment (Calabria, southern Italy) and to map them, using geostatistics, from in-situ  $\gamma$ -ray spectrometry. The activities of naturally occurring radionuclides were measured at 179 locations by *in situ* measurements of  $^{40}\text{K}$ ,  $^{238}\text{U}$ ,  $^{232}\text{Th}$  and total radioactivity and by using gamma-ray spectrometry. Then a multi-Gaussian approach was used to explore and map the activity of naturally occurring radionuclides ( $^{40}\text{K}$ ,  $^{238}\text{U}$ ,  $^{232}\text{Th}$ ) and total radioactivity. Locations and lithological compositions of bedrock appear to be responsible for variations in radioelement activity. From radiometric investigations it has emerged that the natural activity of radionuclides in rocks and soils is not equally distributed, but rather influenced by the different geologic conformations of the various examined areas. As expected, high values of  $^{40}\text{K}$ ,  $^{232}\text{Th}$  and total radioactivity were found in rocks of plutonic origin and low values in sedimentary rocks. Uranium radioactivity behaved in a constant manner in these lithologies, albeit with some differences in clayey sites particularly rich in Uranium.

**Key words:** Radionuclide, Gamma-ray, Multi-Gaussian kriging, Environmental geochemistry, Mineralogy

### INTRODUCTION

Gamma-ray spectrometry survey is an important source of information for soil, regolith, and geochemical studies. It is essentially a radioelement geochemistry technique and its data is a vital sub-component of the geochemical data required for environmental and geological mapping, soil surveying, mineral exploration, and regolith studies. The international geochemical mapping project studied the global inventory of geochemical data and endorsed the significance of radioelement mapping (Darnley *et al.*, 1995).

Radiometric data can be used to tie geochemical data together into a more coherent interpretation when there is some correlation between the radioelements distribution and other measured elements. Radiometric data can be used in planning geochemical surveys because they play a fundamental role in corroborating the interpretation of petrogenetic or pedogenetic associations (IAEA, 2003).

Developing and implementing research into natural radioactivity increases our knowledge about the behaviour of isotopes in natural cycles in particular on the surface environment (Buccianti *et al.*, 2009). In addition, the results obtained in each country can then be exploited to enrich the global data bank, something which is greatly needed in order to evaluate average values of radiometric and dosimetric quantities worldwide (Tzortzis *et al.*, 2003a).

The validity of the *in situ* gamma-ray spectrometry technique for the evaluation of environmental radioactivity has been successfully demonstrated by numerous researches among other Buccianti *et al.* (2009), Frattini *et al.* (2006), Galbraith and Saunders (1983), Hareyama *et al.* (2000), Iqbal *et al.* (2000), Kogan *et al.* (1969), Lee *et al.* (2009).

Gamma-rays are a form of high-energy short-wavelength electromagnetic radiation with no mass or electronic charge and are emitted at different energy

\*Corresponding author E-mail: gabriele.buttafuoco@isafom.cnr.it

levels or peaks that correspond to radioactive decay of particular radioisotopes. The relative abundance or concentration of these radioelements in soil and bedrock is estimated from the intensity of their emission peaks.

Gamma-rays can be separated into primary and secondary sources: primary sources are related to the geochemistry and mineralogy of bedrock, while secondary sources are related to changes or modification of radioelements distribution due to weathering and pedogenesis (Wildford *et al.*, 1997).

Many naturally occurring elements have radioisotopes, but only potassium, and the uranium and thorium decay series have radioisotopes that produce gamma-rays of sufficient energy and intensity to be measured by gamma-ray spectrometry (IAEA, 2003) because they are relatively abundant in the natural environment.

$^{40}\text{K}$  is the radioactive isotope of potassium and occurs as a fixed proportion (0.012%) of natural potassium. This can be used to estimate the total amount of K present (IAEA, 2003).

Uranium occurs naturally as radioisotopes  $^{238}\text{U}$  and  $^{235}\text{U}$ , while thorium occurs as  $^{232}\text{Th}$ . Neither  $^{238}\text{U}$ , nor  $^{232}\text{Th}$  emit gamma-rays and gamma-ray emissions from their radioactive daughters products are used to estimate their concentrations. Statistical analysis of potassium, uranium and thorium contents performed by Kogan *et al.* (1969) for various soil types showed that variations in concentration of these elements in soils of each genetic type, originated from several places, follow an approximate normal distribution. However, this result indicates that the terrestrial gamma-rays emitted by primordial radionuclides, i.e. potassium (K), thorium (Th) and uranium (U), reflect the overall balance between the geological and geographical conditions and the rates of soil production (Minato, 2002; Tzortzis *et al.*, 2003b).

Indeed the content of each of these elements in soils of a particular genetic type is determined by several not very correlated parameters, such as parental rock composition (variations of the radioactive elements in the initial soil-forming rocks) and mineralogy, climate, topography, amount and type of vegetation, water infiltration versus runoff, soil moisture, organic matter, soil types, soil pH, mechanical composition of soils, agricultural practices, impact of fauna and flora, hydrology and so on (Dubois and Bossew, 2003; Anjos *et al.*, 2006; Buccianti *et al.*, 2009). These radionuclides occur virtually in all types of rocks and soils due to geochemical processes which have slowly recycled the crustal material to and from the earth's mantle. For this primary heterogeneity, due to geological and geographical locations, they appear in different levels in rocks in each region in the world (UNSCEAR 2000). Higher radiation levels are

associated with igneous rocks, such as granite, because uranium content of a rock increases with the silica content (Aydin *et al.*, 2006; Zhitkov and Vertman, 2006) and some minerals contain much higher levels of natural radionuclides to others (Ballesteros *et al.*, 2008), and lower levels with sedimentary rocks (Xinwei and Xiaolan, 2008).

In the parent materials for siliciclastic sediments, most of uranium and thorium atoms are bound in accessory and dark-colored minerals (red, purple or black), typically as small highly brittle particles (Anjos *et al.*, 2006). When source rocks disintegrate through weathering and erosion, they are released to accumulate as dark-colored population in sands and other fine-grained deposits. These dark-colored minerals possess higher (by 20–100%) specific weight than the rock-forming minerals (such as quartz and feldspars) and are known as heavy minerals. Consequently, the transport of these heavy minerals is affected by gravitational separation. Generally, Th and U are associated with silt/clay fraction and sesquioxides in soils and tend to concentrate in highly weathered profiles relative to K (Pain *et al.*, 1999). Common heavy mineral suites are composed by zircon, ilmenite, magnetite, garnet, monazite, rutile, and other accessory minerals, some of these enriched in uranium and thorium. Potassium, on the other hand, is abundant in the potash-rich rock-forming minerals, mainly in the orthoclase, also known as the K-feldspar, as well as in accessory heavy minerals. Therefore it is not expected any significant enrichment or depletion of potassium during the transport process. Consequently K is typically high in slightly weathered regolith, depending on bedrock composition, and low in highly weathered regolith due to leaching.

Using gamma-ray spectrometry as a mapping tool requires an understanding of radioelements distribution and mobility. The analysis of spatial variability of radioactivity nuclides is an important technique in many environmental studies to determine their spatial dependence and to carry out a spatial interpolation of sparse measurements and map deposition levels. Characterizing surface spatial heterogeneity is a necessary step in identifying the scale of spatial variation of surface processes structuring the landscape and thus improving their representation in land surface models (Garrigues *et al.*, 2008). Since radioactivity is highly variable in space and time, detailed knowledge of its characteristics is important for understanding and predicting this phenomenon at surface level (Mabit and Bernard, 2007). Gamma-ray measurements can be regarded as regionalized variables (Matheron, 1971) and values at unsampled locations can be predicted using the

geostatistical methods. They provide a valuable tool for studying the spatial structure of radioactivity by taking into account the spatial autocorrelation in data to create mathematical models of spatial correlation structures commonly expressed by variograms. The interpolation technique of the variable at unsampled locations, known as kriging, provides the 'best', unbiased, linear estimate of a regionalized variable in an unsampled location, where 'best' is defined in a least-squares sense (Chilès and Delfiner, 1999; Webster and Oliver, 2007).

## MATERIALS & METHODS

The study area was the Lese catchment which for its geological, lithological and geomorphological characteristics is representative of the Mediterranean environment. The Lese catchment is located in the east-central sector of Calabria along the Ionian slope at east of the Sila Massif and it reverts inside the Crotona Basin. It is a sub-catchment of the larger Neto catchment (Fig. 1). The Crotona Basin is interpreted as a member of the fore arc Ionian Basin, located along the southern border of the Calabrian arc (Amodio-Morelli *et al.*, 1976; Lorenzoni and Zanettin Lorenzoni, 1983). It is bordered by the two zones of cut with orientation NW-SE, Rossano-San Nicola to the north and Petilia-Sosti to the south (Tortorici, 1982; Meulenkamp *et al.*, 1986, Van Dijk, 1990, 1991, Van Dijk and Okkes, 1991 Van Dijk *et al.*, 2000). The study area has rocks from middle-high to low metamorphic degree, Palaeozoic plutonic rocks, Jurassic carbonate rocks, and a sedimentary turbidity succession of Eocene age (Zecchin *et al.*, 2004a; Zecchin *et al.*, 2004b). The lithological outcrop in the study area is mainly represented by a complex of intrusive acid rocks of varying composition: quartz-diorite, quartz-monzonite, granodiorites, and granite and by low to middle degree metamorphites (shale, clayey-schist, phyllites), which present a cleavage from non penetrative to penetrative (Messina *et al.*, 1991; Messina *et al.*, 1994). These include referable terms to the oceanic and continental alpine unities. The fracture and the cleavage are generally very intense. In the most southern part of the basin, sedimentary detritus grounds (mainly pelitic) with subordinate evaporate intervals, are present and they include the deposits of high-Miocene in facies both evaporitic and detritus and the Pliocene sandy, clayey and marl deposits (Sorriso-Valvo and Tansi, 1996). In the most elevated portion of the basin, the modern-day landscape is slightly modified in comparison to the low relief that characterized it before the tectonic lifting at the beginning of the Pleistocene. The morphology of the slopes is controlled by low-rate mass-wasting processes and as result the regolith often reaches a thickness of several tens of meters,

has not been eroded yet (Le Pera *et al.*, 2000; Le Pera *et al.*, 2001). A thick mantle of altered residual products covers the crystalline bedrock of the Lese catchment. The stages of alteration of the rocks of the basement, began in the late Cenozoic-Quaternary, are characterized by different coloration, mineralogical alteration and textural change. The complete profile of the alteration consists of horizons of organic soils on thicker levels of gurus, a crumbled residue of granite formed by hot-and-cold cycling of the daily temperatures, repeated thousands of times, especially on rock that is already weakened from chemical weathering, which alternatively leave uncovered the fresh bedrock below.

The 'radioactive imprint' of rocks makes the radiometric prospecting for lithologic discrimination a useful tool (Lima *et al.*, 2005; Frattini *et al.*, 2006). Rocks irradiate several kinds of ionizing radiation, including alpha, beta and gamma-rays (Hareyama *et al.*, 2000). Unlike alpha and beta particles, gamma-rays are detectable due to the large penetration range (IAEA, 2003).

Only those radionuclides with half-lives comparable to the age of the earth, and their decay products, can still be found today on earth, e.g.  $^{40}\text{K}$ , and the radionuclides from the  $^{238}\text{U}$  and  $^{232}\text{Th}$  series. Potassium, an alkaline element, is both volatile and lithophile so that its concentration in the Earth is poorly constrained. The  $\text{K}^+$  ion is very large and although it may enter octahedral sites, it often fits 12-coordinated sites such as in feldspars and micas and so, as one of the alkali metals, it tends to be concentrated in evolved crystalline rocks such as granites. During melting in the mantle and basalt differentiation, K is markedly incompatible and follows other incompatible elements such as Th and U, thus enriching in felsic igneous melts. The naturally occurring isotopes of potassium are  $^{39}\text{K}$  (93.1%),  $^{40}\text{K}$  (0.0119%) and  $^{41}\text{K}$  (6.9%).  $^{40}\text{K}$  is radioactive with a half-life of  $1.27 \times 10^9$  years, decaying either by K-electron capture or  $\beta$  decay.

Uranium is generally concentrated in the earth crust and there is a relationship between the type of igneous rock and its uranium content (Buccianti *et al.*, 2009). Uranium and Thorium are largely present in the accessory minerals such as zircon, allanite, sphene, monazite, apatite etc. (Mohanty *et al.*, 2004; Vassas *et al.*, 2006; Antal Lundin and Bastani, 2007), and so acid igneous or granitic rocks have the highest concentrations (2-10 mg/kg), basaltic rocks contain lower concentration (0.3-0.8 mg/kg) while the concentrations in sedimentary rocks show a wide range. Thorium is characterised by twenty seven radioisotopes with the most abundant and/or stable being  $^{232}\text{Th}$  with a half-life of about 14.05 billion years. Other important isotopes are  $^{230}\text{Th}$  with a half-life of

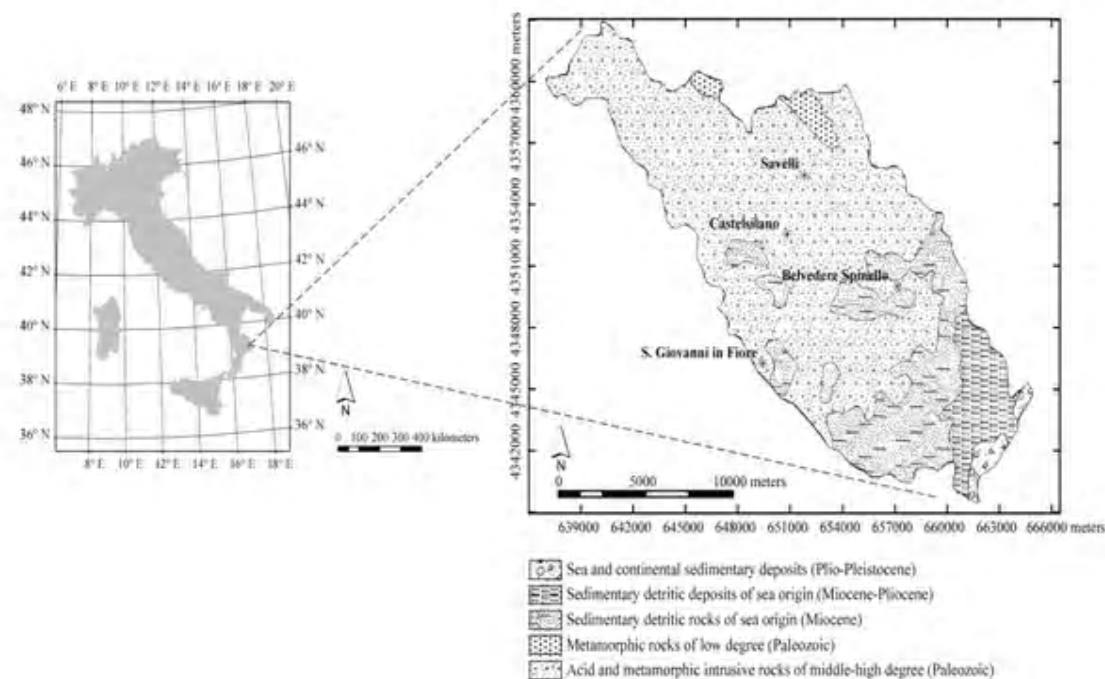


**Fig. 1. Study area location and lithologic map showing the distribution of major rock types in the study area**

75,380 years,  $^{229}\text{Th}$  with a half-life of 7340 years and  $^{228}\text{Th}$  of 1.92 years.

Thorium is a lithophile element, which does not substitute the major elements because of a great difference in ionic radius and ionic charge. A low concentration in the original magma remains in solution and is enriched in the residual liquid of magmatic crystallization (Buccianti *et al.*, 2009).

The concentration of the natural radionuclides in the ground is not equally distributed, but it varies spatially in relation to the different geological conformation of the various areas (Iqbal *et al.*, 2000; Lee *et al.*, 2009). Greater concentrations of radionuclides are found in rocks of volcanic origin and smaller concentrations in sedimentary rocks (Table 1).

In general, concentrations of  $^{238}\text{U}$  in igneous rocks and granites are higher than in sedimentary rocks such as limestone and chalk, even if some sedimentary rocks of marine origin can contain high concentrations of  $^{238}\text{U}$  (Lima *et al.*, 2005). The uranium, as well as thorium, is more abundant in acid rocks than in the basic ones (Aydin *et al.*, 2006; Zhitkov and Vertman, 2006). These rocks contain accessory phases as monazite, allanite and zircon rich of natural radionuclides. Environmental radioactivity can increase significantly in sediments deriving from radioactive eroded rocks.

In order to establish a relation between lithology and the natural gamma radiations, spectra were

**Table 1. Average radioelement content in rocks. Data for U and Th from Taylor (1964, 1966); data for average crustal abundance for K from Weaver and Tarney (1984) and Koljonen (1992), (Lima *et al.*, 2005)**

	$^{40}\text{K}$ (%)	$^{238}\text{U}$ (mg/kg)	$^{232}\text{Th}$ (mg/kg)
Crustal abundance	1.75	2.77	10
Ultramafics	0.50	0.001	0.003
Basalt	0.80	0.6	2.2
Granodiorite	3.30	3	10
Andesite	-	2	-
Granite	3.30	4.8	17
Shale	2.70	4	12
Sandstone	1.10	2.2	-
Limestone	0.30	2	2
Soil	1.40	1	13

collected at locations representing the predominant types of rocks in the Lese catchment. The sampling locations didn't correspond to previously grid established, overlapped on the geological map of study area, because these areas are often poorly accessible for the rough topography (Fig. 2).

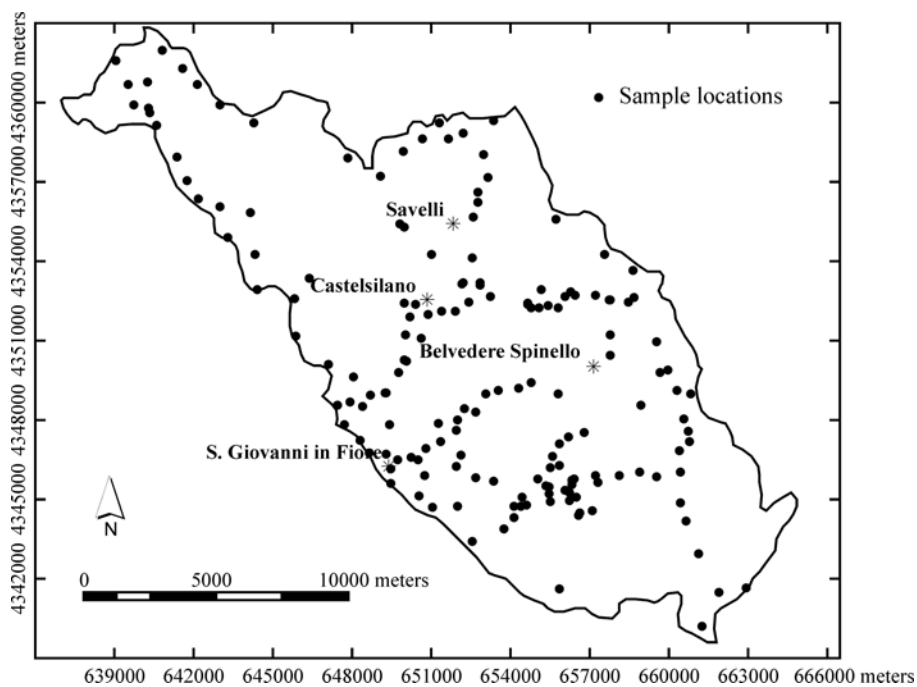


**Fig. 2. Mogan Lake Sampling Points**

Measurements of radioactivity for three natural nuclides  $^{40}\text{K}$ ,  $^{238}\text{U}$ ,  $^{232}\text{Th}$  and total radioactivity in rocks, soils and stream sediments were carried out *in situ* at 179 locations by means of a portable gamma-ray spectrometer GRM-260 of the GF Instruments®. Each measurement included the full spectrum of the natural gamma-radiation (counts per 4 minutes) and registered in 256 channels, each of which equal to 12 keV. The counts were then transformed into activity of the corresponding radioactive elements. The spectrum was divided into four parts, groups of channels called ROI (Region of Interest), in relation to the peak positions of studied radionuclides and due to the resolution of the scintillation detector. The ROI energy borders were 0.401-3.001 MeV for total counts, 1.360-1.558 MeV for  $^{40}\text{K}$ , 1.564-1.953 MeV for  $^{238}\text{U}$  and 2.414-2.804 MeV for  $^{232}\text{Th}$ . The radioactivity measurement was based on the capture of emitted gamma quanta energy in the scintillation detector. The gamma-quanta of characteristic energies were transformed into electric pulses, each of which with a height proportional to its own energy. Therefore the tail of electric pulses was analyzed and separated pulses were gathered in individual channels of the measured spectrum.

$^{40}\text{K}$ ,  $^{238}\text{U}$  and  $^{232}\text{Th}$ , in natural conditions, contain a fraction of a radionuclide that can be detected either directly or indirectly. The isotope  $^{40}\text{K}$  emits gamma-rays with the energy of 1.461 MeV, thus the determination of the potassium was direct. The determination of uranium was indirect because it is

based on the detection of the  $^{214}\text{Bi}$  radionuclide, which is a member of  $^{238}\text{U}$  decay series emitting the energy of 1.764 MeV. Also the determination of  $^{232}\text{Th}$  contents was indirect and based on the measurement of the radionuclide  $^{208}\text{Tl}$ , which emits energy of 2.615 MeV, originating from the  $^{232}\text{Th}$  decay series.

The  $^{40}\text{K}$  concentration was measured in mass percentage (%) because of its higher crustal abundance, while  $^{238}\text{U}$  and  $^{232}\text{Th}$  in equivalent parts per million (eU and eTh), which indicates that their concentrations were inferred from daughter elements in their decay chains. The dose rate values were given in nGy/h and automatically can be recalculated in U, unity of equivalent concentration (the unity dose rate of 1 U corresponds to 1 mg/kg of concentration of U). The accuracy of the measurements was provided by the system of spectrum stabilization through the use of a digital circuitry. The factory calibration of the gamma-ray spectrometer was made to high volume standards (etalons) for each element  $^{238}\text{U}$ ,  $^{232}\text{Th}$  and  $^{40}\text{K}$  and for background.

Furthermore, in order to test the statistical variations associated with the process of counting, two samples from the same site were measured. These replicate measurements provided accuracy and precision < 5%.

To make a geochemical judgment regarding the relative favorability of a formation as a source rock for  $^{238}\text{U}$ ,  $^{232}\text{Th}$  and  $^{40}\text{K}$  activity, one must first determine

the rock's type and then whether it is depleted or enriched in  $^{238}\text{U}$ ,  $^{232}\text{Th}$  and  $^{40}\text{K}$  with respect to the normal, or average, abundance for that rock type (Galbraith and Saunders, 1983). For this, in order to identify the mineralogical radioactive sources, some representative rock samples were selected and in detail characterized.

The mineralogical composition of the samples was investigated by:

- i) X-Ray Powder Diffraction (XRPD) with a Philips PW 1730 diffractometer equipped with Cu-K $\alpha$  radiation, operating at 40 kV and 20 mA. Powder diffraction data were collected in the range from  $4^\circ$  to  $60^\circ$   $2\theta$  with steps of  $0.02^\circ$   $2\theta$ , (time step 0.4 s). The EVA software program was used to determine the mineral phases present in each X-ray powder spectrum, by comparing the experimental peaks with PDF2 reference patterns.
- ii) Secondary electron SEM images with annexed EDS electron microprobes for chemical analyses were performed by a FEI Quanta 200 equipped with a field emission gun (FEG).

Samples were sieved and single crystals selected under a binocular microscope, subsequently cleaned by sonication in hot water for 10 minutes. Finally, single crystals were studied under a microscope (SEM-EDS) to identify the different mineralogical phases.

A geostatistical approach was used to analyse and map the spatial structure of radiometric data. In Geostatistics each measured value,  $z(\mathbf{x}_\alpha)$ , at location  $\mathbf{x}_\alpha$  ( $\mathbf{x}$  is the location coordinates vector and  $\alpha = 1, \dots, n$  is the sampling points) is interpreted as a particular realization, or outcome, of a random variable  $Z(\mathbf{x}_\alpha)$ . The set of dependent random variables  $\{Z(\mathbf{x}_\alpha), \alpha = 1, \dots, n\}$  constitutes a random function  $Z(\mathbf{x})$ . For a detailed presentation of the theory of random functions, interested readers should refer to as the works of Journel and Huijbregts (1978), Isaaks and Srivastava (1989), Goovaerts (1997), Chilès and Delfiner (1999), Webster and Oliver (2007), Wackernagel (2003), among others.

An important tool in geostatistics is the experimental variogram, which is a quantitative measure of spatial correlation of the regionalized variable  $z(\mathbf{x}_\alpha)$ . The experimental variogram  $\gamma(\mathbf{h})$  is a function of the lag  $\mathbf{h}$ , a vector in distance and direction, of data pair values  $[z(\mathbf{x}_\alpha), z(\mathbf{x}_\alpha + \mathbf{h})]$ ; it refers to the expected value of the squared differences; a way of calculating this is reported in Eq. (1):

$$\gamma(\mathbf{h}) = \frac{1}{2N(\mathbf{h})} \sum_{\alpha=1}^{N(\mathbf{h})} [z(\mathbf{x}_\alpha) - z(\mathbf{x}_\alpha + \mathbf{h})]^2 \quad (1)$$

where  $N(\mathbf{h})$  is the number of data pairs for the specified lag vector  $\mathbf{h}$ . A theoretical function, known as the variogram model, is fitted to the experimental variogram to allow one to estimate the variogram analytically for any distance  $\mathbf{h}$ . The function used to model the experimental variogram must be conditionally negative definite to ensure that the kriging variances are positive (see later Eq. 9). The aim is to build a model that describes the major spatial features of the attribute under study. The models used can represent bound or unbound variation. In the former models the variance has a maximum (known as the sill variance) at a finite lag distance (range) over which pairs of values are spatially correlated. The best fitting function can be chosen by cross-validation, which checks the compatibility between the data and the model. It takes each data point in turn, removing it temporarily from the data set and using its neighboring information to predict the value of the variable at its location. The estimate is compared with the measured value by calculating the experimental error, i.e. the difference between estimate and measurement, which can also be standardized by estimating the standard deviation. The goodness of fit was evaluated by the mean error and the mean squared deviation ratio. The mean error (ME) proves the unbiasedness of the estimate if its value is close to 0:

$$ME = \frac{1}{n} \sum_{\alpha=1}^n [z^*(\mathbf{x}_\alpha) - z(\mathbf{x}_\alpha)] \quad (2)$$

where  $n$  is the number of observation points,  $z^*(\mathbf{x}_\alpha)$  is the predicted value at location  $\mathbf{x}_\alpha$ , and  $z(\mathbf{x}_\alpha)$  is the observed value at location  $\mathbf{x}_\alpha$ . The mean squared deviation ratio (MSDR) is the ratio between the squared errors and the kriging variance  $\sigma^2(\mathbf{x}_\alpha)$ :

$$MSDR = \frac{1}{n} \sum_{\alpha=1}^n \frac{[z^*(\mathbf{x}_\alpha) - z(\mathbf{x}_\alpha)]^2}{\sigma^2(\mathbf{x}_\alpha)} \quad (3)$$

If the model for the variogram is accurate, the mean squared error should equal the kriging variance and the MSDR value should be 1.

After selecting an appropriate variogram model, the parameters can be used with the data to predict radioactivity at unsampled locations using a kriging algorithm.

Geostatistical methods are most efficient when carried out on variables that have Gaussian distributions, because a few exceptionally large or small values may contribute to several squared differences and inflate the average variance (Webster and Oliver, 2007). The choice of a kriging algorithm from the ones available should be primarily guided by the characteristics of the data under study. For skewed data in the 1970s, mining geostatisticians developed lognormal kriging to cope with the presence of a few high grades (Roth, 1998). The technique was developed to reduce the influence of few high values and kriging is applied to lognormal transforms of data followed by a back-transformation of final estimates (Dowd, 1982; Roth, 1998). However, lognormal kriging must be used with caution because it is non robust to departures from the lognormal model and the back-transformation is very sensitive to variogram fluctuations (Roth, 1998). Rivoirard (1990) provided a review of the different lognormal estimators. Gaussian anamorphosis (Chilès and Delfiner, 1999; Wackernagel, 2003) is a more flexible approach when the experimental distribution of skewed data departs from the lognormal model. Each measured radiometric variable  $\{Z(\mathbf{x}), \mathbf{x} \in R^2\}$  was transformed into a Gaussian-shaped variable  $\{Y(\mathbf{x}), \mathbf{x} \in R^2\}$  with zero mean and unit variance, such that:

$$Z(\mathbf{x}) = \phi[Y(\mathbf{x})] \tag{4}$$

Such a procedure is a mathematical function which transforms a variable  $Y$  with a Gaussian distribution in a new variable with any distribution. To transform the raw variable into a Gaussian one, we have to invert this function:

$$Y(\mathbf{x}) = \phi^{-1}[Z(\mathbf{x})] \tag{5}$$

The Gaussian anamorphosis can be achieved by using an expansion into Hermite polynomials  $H_i(Y)$  (Wackernagel, 2003; Bleines *et al.*, 2008) restricted to a finite number of terms:

$$\phi(Y) = \sum_{i=0}^n \psi_i H_i(Y) \tag{6}$$

The modelling of the anamorphosis starts with the discrete version of the curve on the true data set; then a model expanded in terms of Hermite polynomials (Eq. 6) is fitted to the discretized anamorphosis. This model gives the correspondence between each one of the

sorted raw data and the corresponding frequency quantile in the standardized Gaussian scale. For a detailed description of the Hermite polynomials, interested readers should refer to Chilès and Delfiner (1999), Webster and Oliver (2007), Wackernagel (2003). The kriging of such normalized data is referred to as multi-Gaussian kriging (Verly, 1983; Goovaerts, 1997; Wackernagel, 2003). In the multi-Gaussian approach we can choose between simple and ordinary kriging. Unlike simple multi-Gaussian kriging, such as disjunctive kriging (Matheron, 1976), ordinary multi-Gaussian kriging accounts for the local mean calculated after the data located in the kriging neighbourhood (Emery, 2005). The use of ordinary kriging in the multi-Gaussian approach leads to a weakening of the stationary assumption when using non linear geostatistical methods and makes it robust to a departure of the data from the ideal stationary model. The transformed data are used for interpolation at all unsampled locations as a linear combination of  $n(\mathbf{x}_0)$  Gaussian data surrounding the unsampled point  $(\mathbf{x}_0)$  using the following expression:

$$y_{MK}^*(\mathbf{x}_0) = \sum_{\alpha=1}^{n(\mathbf{x}_0)} \lambda_{\alpha}^{MK}(\mathbf{x}_0) y(\mathbf{x}_{\alpha}) \tag{7}$$

The key issue is the determination of the weights  $\lambda_{\alpha}^{MK}(\mathbf{x})$  assigned to each sample. The kriging weights are chosen so as to minimize the estimation variance  $\sigma_E^2(\mathbf{x}) = Var[Y^*(\mathbf{x}) - Y(\mathbf{x})]$  under the constraint of unbiasedness that  $E[Y^*(\mathbf{x}) - Y(\mathbf{x})] = 0$ . The kriging weights are calculated by solving the following system of linear equations:

$$\left\{ \begin{array}{l} \sum_{\beta=1}^{n(\mathbf{x})} \lambda_{\beta}^{MK}(\mathbf{x}) \gamma(\mathbf{x}_{\beta} - \mathbf{x}_{\alpha}) - \mu(\mathbf{x}) = \gamma(\mathbf{x} - \mathbf{x}_{\alpha}) \quad \alpha = 1, \dots, n(\mathbf{x}) \\ \sum_{\beta=1}^{n(\mathbf{x})} \lambda_{\beta}^{MK}(\mathbf{x}) = 1 \end{array} \right. \tag{8}$$

and the kriging variance is:

$$\sigma_{MK}^2(\mathbf{x}) = \sum_{\alpha=1}^{n(\mathbf{x})} \lambda_{\alpha}^{MK}(\mathbf{x}) \gamma(\mathbf{x} - \mathbf{x}_{\alpha}) - \mu(\mathbf{x}) \tag{9}$$

The unbiasedness of the estimator is ensured by constraining the weights to sum to one, which requires the definition of the Lagrange parameter  $\mu(\mathbf{x})$ .

Finally, the values of the Gaussian variable were estimated at the nodes of a 50 m x 50 m interpolation grid and back-transformed using the inverse Gaussian anamorphosis (Eq. 4).

**RESULTS & DISCUSSION**

The descriptive statistics of the radioactivity values are presented in Table 2. The radioactivity ranged from 0.86 to 7.98 Bq for potassium-40, from 0.37 to 8.54 Bq for uranium-238, from 0.07 to 1.14 Bq for thorium-232 and from 329.56 to 489.26 Bq for total radioactivity. The distributions of the total and uranium-238 radioactivity values were positively skewed with values of 0.76 and 1.64 (Table 2). Moreover, the two distributions were more peaked than normal with a kurtosis of 4.48 and 5.78 (Table 2). Webster and Oliver (2007) suggest no Gaussian transformation with skew positive between 0 and 0.5, a square root transformation with skew values between 0.5 and 1, and a logarithm transformation for skew values greater than 1. We preferred to transform all the radioactivity values to normality by using a Gaussian anamorphosis by an expansion of Hermite polynomials restricted to the first 30 terms (Wackernagel, 2003). Therefore, all calculations were performed on the Gaussian transformed variables.

No anisotropy was evident in the maps of the 2-D variograms (not shown) to a maximum lag distance of 15 km. To fit the shape of the experimental variograms (Fig. 3) two basic structures were combined (nested) (Table 3) including a nugget effect ( $c_0$ ) and a spherical model (*Sph*) for G <sup>238</sup>U (range = 8177 m) and G Total radioactivity (range = 7057 m), while for G <sup>40</sup>K and G <sup>232</sup>Th, the basic structures (Table 3) included a nugget effect ( $c_0$ ) and an exponential model (*Exp*). The ranges of exponential model were 7660 m for G <sup>40</sup>K and 8170 m for G <sup>232</sup>Th. As can be seen from the variograms there is a spatial correlation of radioactivity up to about 7000-8000 m for the three nuclides and the total radioactivity.

The nugget effect implies a discontinuity in  $\gamma$  and is a positive intercept of the variogram. It arises from errors of measurement and spatial variation within the shortest sampling interval (Webster and Oliver, 2007). The spherical model (Webster and Oliver, 2007) is given by:

$$\gamma(h) = \begin{cases} c \left[ \frac{3h}{2a} - \frac{1}{2} \left( \frac{h}{a} \right)^3 \right] & \text{if } h \leq a \\ c & \text{if } h > a \end{cases} \quad (10)$$

where  $c$  is the sill and  $a$  the range. The ratio of nugget effect to total semivariance is about 0.28 for Uranium-238 and 0.06 for total radioactivity. These ratio values indicate a marked spatial dependence (Cambardella *et al.*, 1994).

The exponential model (Webster and Oliver, 2007) is given by:

$$\gamma(h) = c \left[ 1 - \exp\left(-\frac{h}{r}\right) \right] \quad (11)$$

where  $c$  is the sill and  $r$  is a distance parameter defining the spatial extent of the model. The exponential model approaches its sill asymptotically, thus it does not have a finite range  $a$ . For practical purposes it can be assigned an effective range, and this is taken as the distance at which  $\gamma$  is equal to 95% of the sill variance, approximately  $3r$ .

The ratio of nugget effect to total semivariance is about 0.35 for potassium-40 and 0.42 for thorium-232. These ratio values indicate less spatial dependence for thorium than the other analyzed variants. The goodness of fit was checked by cross validation and the results were quite satisfactory, because the statistics used, i.e. mean of the raw estimation errors, were quite close to 0, while the variance of the

**Table 2. Basic statistics of activity for <sup>40</sup>K, <sup>238</sup>U, <sup>232</sup>Th and total radioactivity**

	Total radioactivity	<sup>40</sup> K	<sup>238</sup> U	<sup>232</sup> Th
Minimum (Bq)	329.56	0.86	0.37	0.07
Mean (Bq)	376.20	3.44	2.11	0.52
Median (Bq)	372.73	3.51	1.56	0.54
Maximum (Bq)	489.26	7.98	8.54	1.14
Std. Dev. (Bq)	25.34	1.32	1.51	0.21
Variat.Cof. (-)	0.07	0.38	0.72	0.41
Skewness (-)	0.76	0.23	1.64	-0.17
Kurtosis (-)	4.48	3.12	5.78	2.83

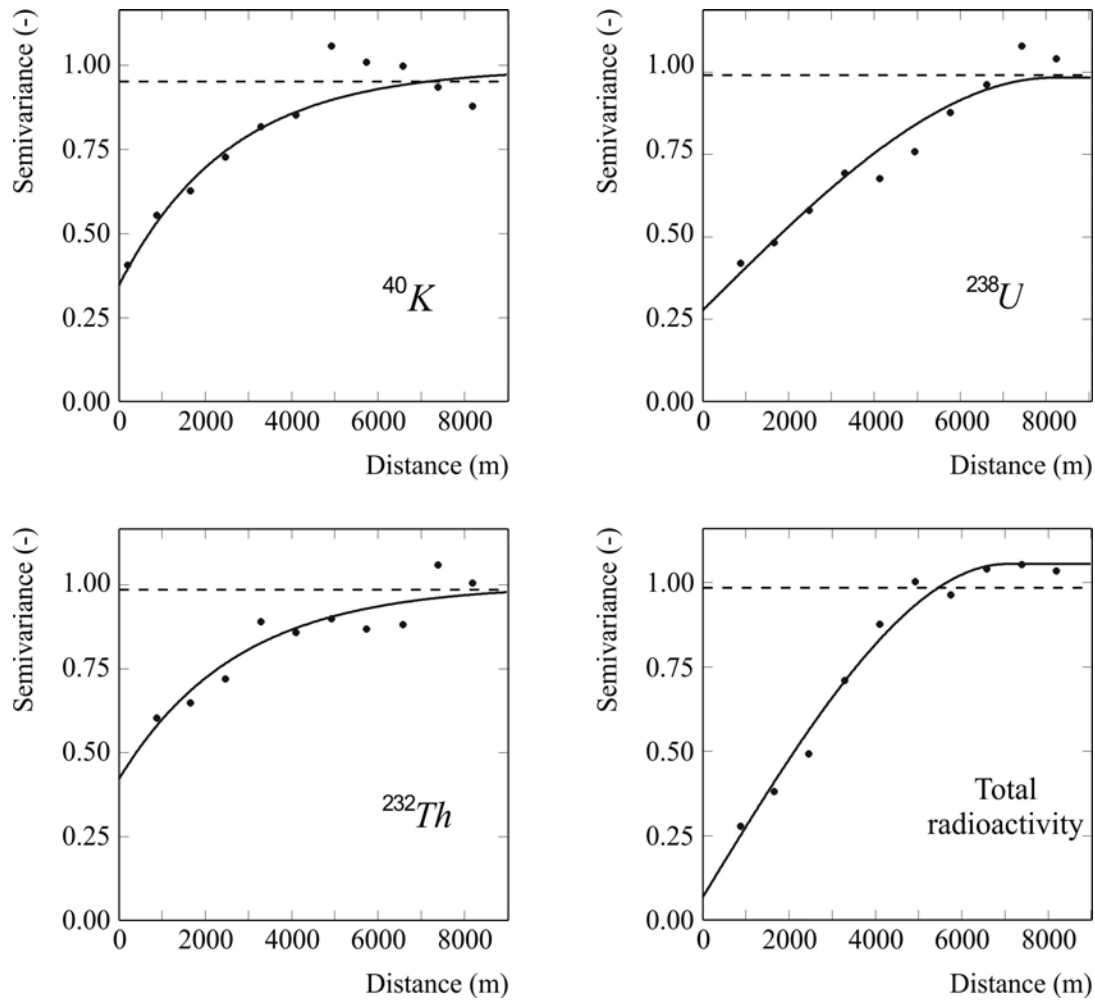


Fig. 3. Comparison of the Dissolved Oxygen, Suspended Solid Substances, Temperature, pH, Total Nitrogen and Total Phosphorus Measured values and the Model Outputs for 2004

Table 3. Variogram model parameters deviations for Gaussian data activity of  $^{40}\text{K}$ ,  $^{238}\text{U}$ ,  $^{232}\text{Th}$  and total radioactivity

Variable	Model	Range (m)	Sill (-)
G $^{40}\text{K}$	Nugget	-	0.3459
	Exponential	7660 <sup>a</sup>	0.6455
G $^{238}\text{U}$	Nugget	-	0.2773
	Spherical	8177	0.7057
G $^{232}\text{Th}$	Nugget	-	0.4217
	Exponential	8170 <sup>a</sup>	0.5780
G Total radioactivity	Nugget	-	0.0684
	Spherical	7057	0.9865

<sup>a</sup>Practical range equal to  $3r$

standardized error ranged between 0.92 and 1.20 (Table 4). The interpretation of gamma-ray spectrometry data in terms of lithology can be generally difficult. With the exception of some granites and types of alteration, rock classification schemes do not typically accommodate radioelement content. The interpreter must therefore rely on a correlation with known geology to develop the lithological framework (IAEA, 2003). In terms of natural radioactivity, granitic rocks exhibit an enhanced elemental concentration of uranium-238 and thorium-232 compared to the very low abundance of these elements observed in the mantle and the crust of the Earth. Certain minerals, such as zircon and monazite, which form as common trace constituents in igneous rocks, have crystal structures which can accommodate varying amounts of the naturally occurring radioactive elements, uranium and thorium.

**Table 4. Results of cross validation test performed for activity of  $^{40}\text{K}$ ,  $^{238}\text{U}$ ,  $^{232}\text{Th}$  and total radioactivity**

Variable	Mean Error	Mean squared deviation ratio
G $^{40}\text{K}$	0.0311	0.92
G $^{238}\text{U}$	0.0622	1.02
G $^{232}\text{Th}$	0.0075	1.08
G Total radioactivity	0.0300	1.22

A presumable explanation of this behavior is provided in the course of partial melting and fractional crystallization of magma, which enables U and Th to be concentrated in the liquid phase and become incorporated into the more silica-rich products. The radioelement concentrations show an increase in average radioelement concentration with an increase of  $\text{SiO}_2$ . For thorium and uranium this is due to the high

charge and radius of the  $\text{Th}^{4+}$  and  $\text{U}^{4+}$  ions, which excludes them in the substitution of major ions in the crystallization of early rock forming minerals. U appears in the valence state  $\text{U}^{4+}$  in igneous rocks with crystal-chemical properties close to  $\text{Th}^{4+}$  and the Light Rare Earth Elements (LREE), which explains the coherent geochemistry of U, Th and LREE in igneous rocks (Bea, 1999). For that reason, igneous rocks of granitic composition are strongly enriched in U and Th which accommodated in accessory minerals (zircon, allanite, and monazite). Mostly zircon has a radioactive nature due to its content of uranium/thorium and is not affected by low temperature processes found on the earth surface. Consequently the uranium and thorium in zircon is that given it during crystallisation from the melt. The nature of the zircon crystal inhibits the removal of uranium and thorium and is one of the properties that allow this mineral to be used for mapping radioactivity in rocks.

Zircon occurs naturally associated with quartz and other minerals, such as rutile ( $\text{TiO}_2$ ), ilmenite ( $\text{FeTiO}_3$ ) and monazite (phosphate of rare earth). In addition these accessory minerals are the most resistant to weathering. The analysis revealed the perfect agreement between the geochemical behaviour of radionuclides analyzed and their variogram models. The spatial distribution of the described radionuclides can be explained fairly satisfactorily by considering the geochemical behaviour. The enrichment of  $^{238}\text{U}$  and  $^{232}\text{Th}$  in the intrusive rocks is easily explained by their concentration at the felsic end of the series, hosted in minerals such as zircon and monazite, due to their smaller radii and mostly higher charges. The possible explanation for the generally slight enrichment of  $^{238}\text{U}$  in clays and fine-grained fluvial sediments is that U in

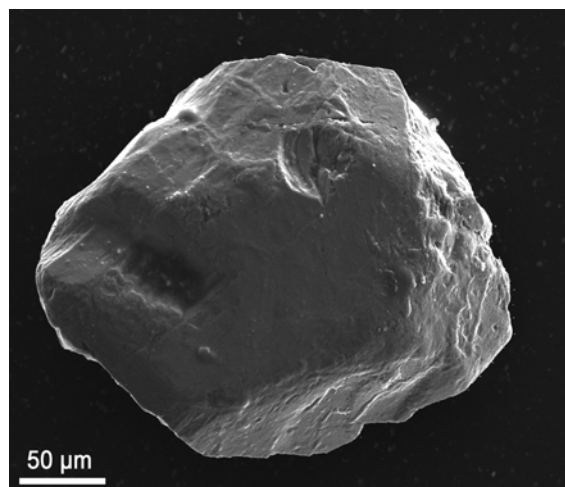


**Fig. 4. Secondary electron SEM image of monazite single crystal**

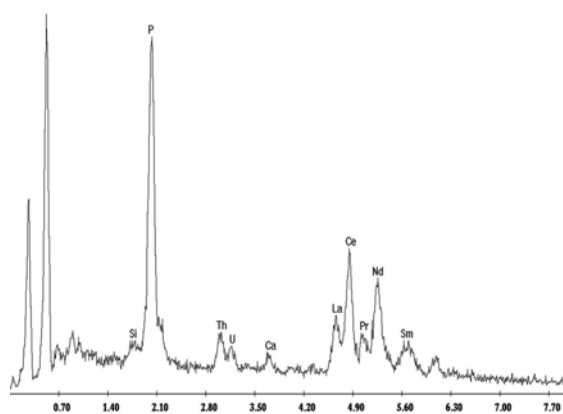


**Fig. 5. EDX spectra of monazite**

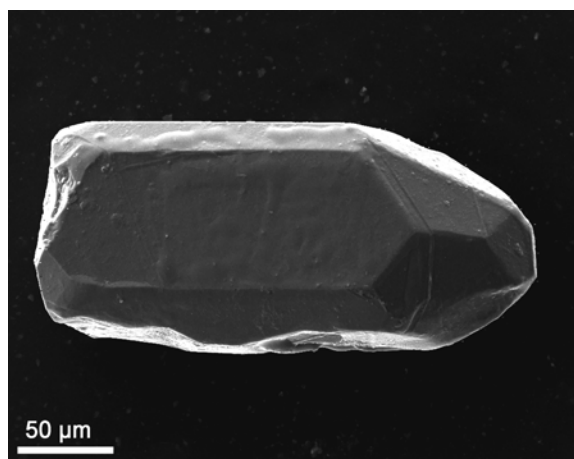


Fig. 6. Secondary electron SEM image of zircon single crystal

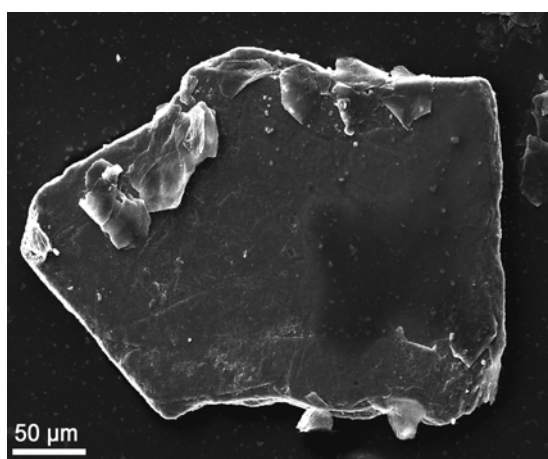


Fig. 7. Secondary electron SEM image of biotite single crystal

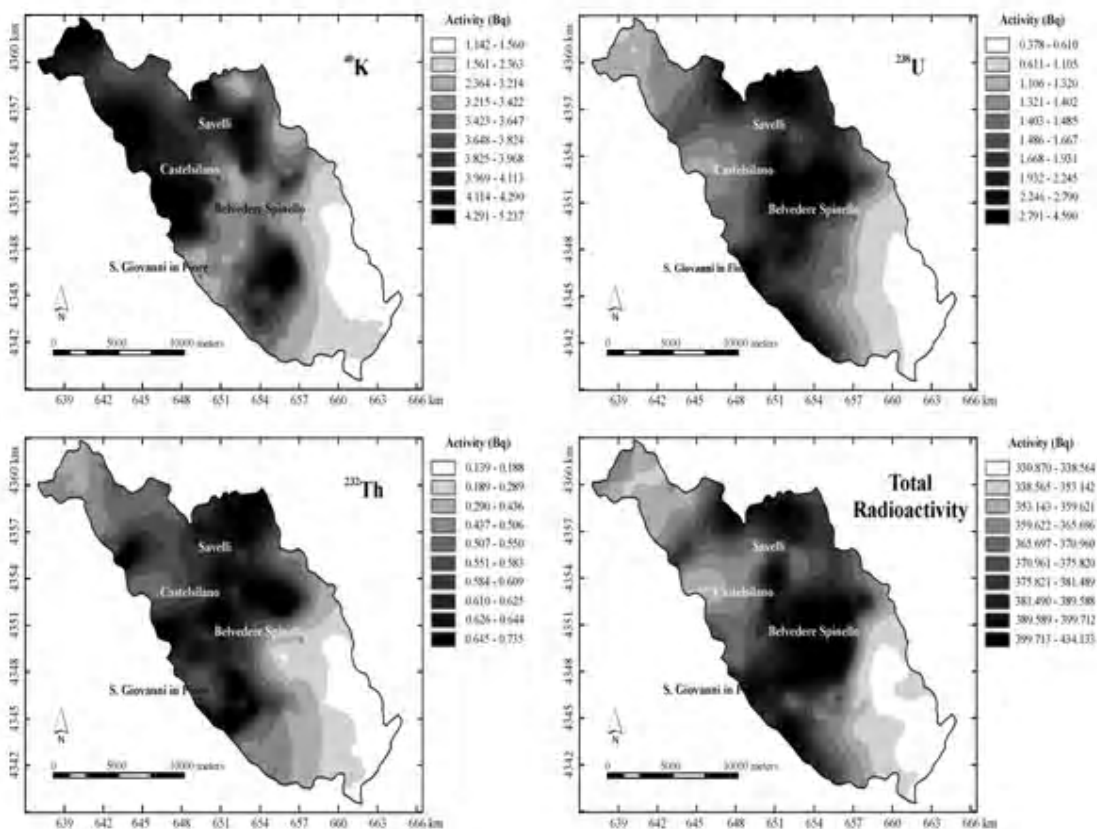


Fig. 8. Maps of predicted activity of  $^{40}\text{K}$ ,  $^{238}\text{U}$ ,  $^{232}\text{Th}$  and total radioactivity

respect to  $^{232}\text{Th}$  is mobile in oxidized conditions; it can be mobilized in aqueous solutions and may be precipitated with clay as hydroxides or complex minerals of uranium in the hexa-valent state. XRPD showed that samples were mainly composed of quartz, K-feldspar, plagioclase, pyroxene, chlorite, mica (biotite, muscovite), hornblende. Although a wide variety of

single crystals (*i.e.*, ilmenite, apatite, granato, rutile, magnetite, hematite) was identified, only REE-phosphates (monazite-type), zircon often rich in  $^{232}\text{Th}$  and  $^{238}\text{U}$  (Figs 4, 5 and 6), biotite rich in  $^{40}\text{K}$  (Fig. 7) and K-feldspar can be retained as potential sources of radioactivity.

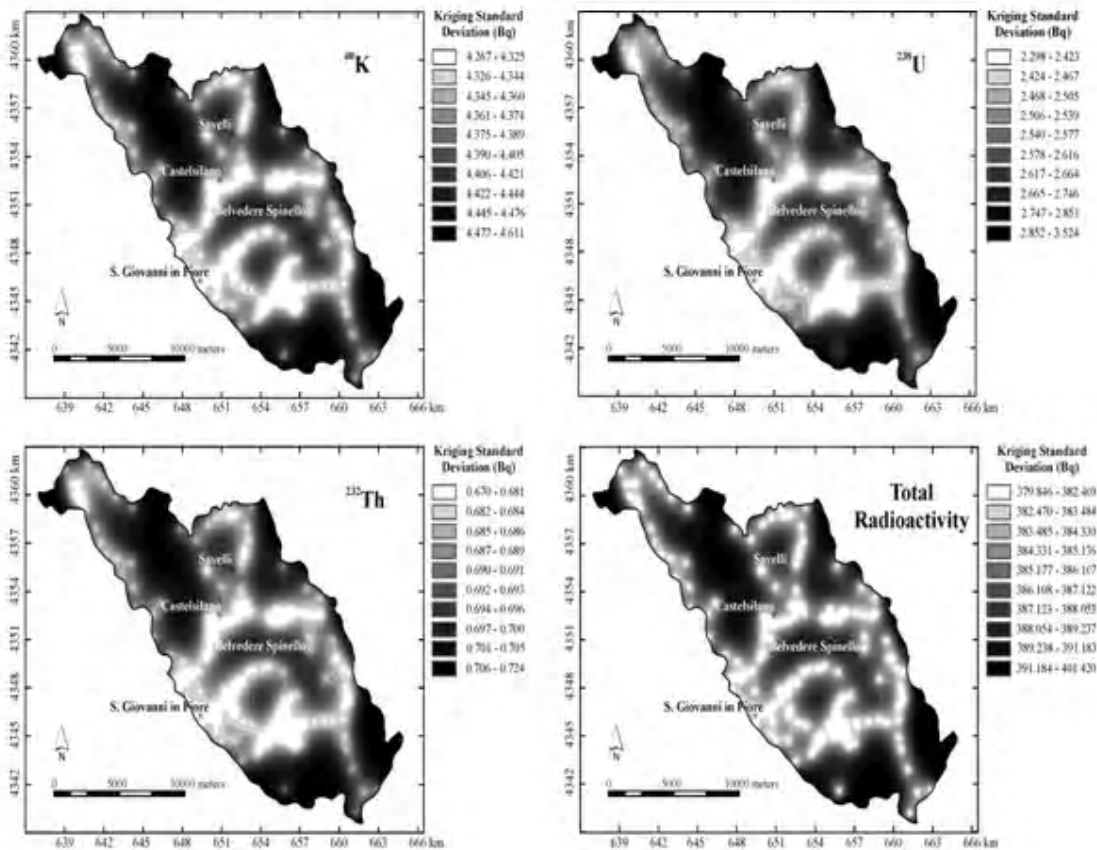


Fig. 9. Maps of kriging standard deviations of  $^{40}\text{K}$ ,  $^{238}\text{U}$ ,  $^{232}\text{Th}$  and total radioactivity

## CONCLUSION

Gamma-spectrometry measurements were carried out in representative sites of the Lese catchment in order to sample radioactivity; the aim of this work was to provide information on regolith properties including mineralogy and chemistry by gamma-ray responses and so to detect the influence of bedrock composition on the radioactive concentrations. The data provided an identification of radiometric anomalies and a finding of the relation between terrestrial radiation and the nature of the rock, by studying dose contributions of each natural series,  $^{232}\text{Th}$ ,  $^{238}\text{U}$ , and  $^{40}\text{K}$  that occur with different activities on rock composition. The multi-Gaussian approach allowed to explore the spatial structure and to quantify the spatial dependence of the radiation levels. This approach also led to the identification of hotspots of radioactivity in the soil. Moreover, the rough exploration of the relationship between lithology and radioactivity has showed that natural radionuclide activity in rocks and soils is not equally distributed, but varies according to the different geological conformations of the areas examined. High values of  $^{40}\text{K}$ ,  $^{232}\text{Th}$  and total radioactivity were found in rocks of plutonic origin and low activity values in sedimentary rocks (not deriving from magmatic rocks). Uranium radioactivity behaved in a uniform manner,

albeit with some differences in clayey sites particularly rich in uranium. In addition, this work has shown gamma radiation surveying to be an accurate, rapid and inexpensive technique for exploring environmental matrices. In particular, it proved to be a useful and reliable method for obtaining real information on radionuclides in the environment and can also be utilized in the assessment of the lithological composition of the rocks and mineralogical phases.

## ACKNOWLEDGEMENTS

The authors thank the reviewers of this paper for providing constructive comments which have contributed to improve the published version.

## REFERENCES

- Amodio-Morelli, L., Bonardi, G., Colonna, V., Dietrich, D., Giunta, G., Ippolito, F., Liguori, V., Lorenzoni, S., Paglionico, A., Perrone, V., Piccarreta, G., Russo, M., Scandone, P., Zanettin-Lorenzoni, E. and Zuppetta, A. (1976). L'arco calabro-peloritano nell'orogene appenninico-maghrèbide. *Memorie della Società Geologica Italiana*, **17**, 1–60.
- Anjos, R.M., Veiga, R., Macario, K., Carvalho, C., Sanches, N., Bastos, J. and Gomes, P. R. S. (2006). Radiometric analysis of Quaternary deposits from the southeastern Brazilian coast. *Marine Geology*, **229**, 29–43.

- Antal Lundin, I. and Bastani, M. (2007). Analysis of petrophysical properties of some granitoids in Sweden. *Journal of Applied Geophysics*, **62**, 74–87.
- Aydin, I., Aydođan, M. S., Oksum, E. and Koçak, A. (2006). An attempt to use aerial gamma-ray spectrometry results in petrochemical assessments of the volcanic and plutonic associations of Central Anatolia (Turkey). *Geophysical Journal International*, **167**, 1044–1052.
- Ballesteros, L., Zarza, I., Ortiz, J. and Serradell, V. (2008). Occupational exposure to natural radioactivity in a zircon sand milling plant. *Journal of Environmental Radioactivity*, **99**, 1525–1529.
- Bea, F. (1999). Uranium. In C.P. Marshall and R.W. Fairbridge (Eds.), *Encyclopedia of Geochemistry*, (pp.712). London: Kluwer Academic Publishers.
- Bleines, C., Deraisme, J., Geoffrey, F., Jeannée, N., Perseval, S., Rambert, F., Renard, D., Torres, O. and Touffait, Y. (2008). *Isatis Software Manual*, 5th Edition. Géovariances & Ecole des Mines de Paris, Avon.
- Buccianti, A., Apollaro, C., Bloise, A., De Rosa, R., Falcone, G., Scarciglia, F., Tallarico, A. and Vecchio, G. (2009). Natural radioactivity levels (K, Th, U and Rn) in the Cecita Lake area (Sila Massif, Calabria, Southern Italy): An attempt to discover correlations with soil features on a statistical base. *Geoderma*, **152**, 145–156.
- Cambardella, C. A., Moorman, T. B., Novak, J. M., Parkin, T. B., Karlen, D. L., Turco, R. F., Konopka, A. (1994). Field-scale variability of soil properties in central Iowa soils. *Soil Science Society of America Journal*, **58**, 1501"1511.
- Chilès, J. P. and Delfiner, P. (1999). *Geostatistics: Modelling Spatial Uncertainty*. New York: Wiley.
- Darnley, A. G., Björklund, A., Bølviken, B., Gustavsson, N., Koval, P. V., Plant, J. A., Steenfelt, A., Tauchid, M. and Xie, X. (1995). A global geochemical database for environmental and resource management. *Earth Sciences* 19, Paris: United Nations Educational, Scientific and Cultural Organization.
- Dowd, P. A. (1982). Lognormal kriging - The general case. *Mathematical Geology*, **14**, 474–500.
- Dubois, G. and Bossew, P. (2003). Spatial analysis of <sup>137</sup>Cs in the environment: an overview on the current experience. (In: G. Dubois, J. Malczewski, M. De Cort (Eds.), *Mapping radioactivity in the environment*. (pp 21–36). *Spatial Interpolation Comparison* 97.
- Emery, X. (2005). Simple and Ordinary Multigaussian Kriging for Estimating Recoverable Reserves. *Mathematical Geology*, **37**, 295"319.
- Fratini, P., De Vivo, B., Lima, A. and Cicchella, D. (2006). Elemental and gamma-ray surveys in the volcanic soils of Ischia Island (Italy). *Geochemistry: Exploration, Environment, Analysis*, **6**, 325–339.
- Galbraith, J. H. and Saunders, D. F. (1983). Rock classification by characteristics of aerial gamma-ray measurements. *Journal of Geochemical Exploration*, **18**, 49–73.
- Garrigues, S., Allard, D., Baret, F. and Morissette, J. (2008). Multivariate quantification of landscape spatial heterogeneity using variogram models. *Remote Sensing of Environment*, **112**, 216–230.
- Goovaerts, P. (1997). *Geostatistics for Natural Resources Evaluation*. Oxford University Press, New York.
- Hareyama, M., Tsuchiya, N., Takebe, M. and Chida, T. (2000). Two-dimensional measurement of natural radioactivity of granitic rocks by photostimulated luminescence technique. *Geochemical Journal*, **34**, 1–9.
- IAEA, (2003). *Guidelines for radioelement mapping using gamma ray spectrometry data*. (IAEA-TECDOC-1363, Vienna: International Atomic Energy Agency.
- Iqbal, M., Tufail, M. and Mirza, S. M. (2000). Measurement of natural radioactivity in marble found in Pakistan using a NaI(Tl) gamma-ray spectrometer. *Journal of Environmental Radioactivity*, **51**, 255–265.
- Isaaks, E. H. and Srivastava, R. M. (1989). *Applied Geostatistics*. New York: Oxford University Press.
- Journel, A. G. and Huijbregts, C. J. (1978). *Mining Geostatistics*. (San Diego: Academic Press).
- Kogan, R. M., Nazarov, L. M. and Fridman, Sh. D. (1969). *Gamma Spectrometry of Natural Environments and Formations*. Moscow: Moskva Atomizdat.
- Koljonen, T. (1992). *The Geochemical Atlas of Finland, Part 2: Till*. (Espoo, Finland: Geological Survey of Finland.
- Le Pera, E., Arribas, J., Critelli, S. and Tortosa, A. (2001). The effects of source rocks and chemical weathering on the petrogenesis of siliciclastic sand from the Neto River (Calabria, Italy): implications for provenance studies. *Sedimentology*, **48**, 357–378.
- Le Pera, E., Mongelli, G., Morelli, F. and Critelli, S. (2000). Petrographical and geochemical signature of provenance in modern sediments from the Tyrrhenian continental shelf, Calabria, Italy. *Giornale di Geologia*, **62**, 37–55.
- Lee, S. K., Wagiran, H., Ramli, A. T., Apriantoro, N. H. and Wood, A. K. (2009). Radiological monitoring: terrestrial natural radionuclides in Kinta District, Perak, Malaysia. *Journal of Environmental Radioactivity*, **100**, 368–374.
- Lima, A., Albanese, S. and Cicchella, D. (2005). Geochemical baselines for the radioelements K, U and Th in the Campania region, Italy: a comparison of stream-sediment geochemistry and gamma-ray surveys. *Applied Geochemistry* **20**, 611–625.
- Lorenzoni, S. and Zanettin Lorenzoni, E. (1983). Note illustrative della carta geologica della Sila alla scala 1:200.000. *Memorie di Scienze Geologiche già Memorie degli Istituti di Geologia e Mineralogia dell'Università di Padova*, vol XXXVI, 317–342,.
- Mabit, L. and Bernard, C. (2007). Assessment of spatial distribution of fallout radionuclides through geostatistics concept. *Journal of Environmental Radioactivity*, **97**, 206–219.
- Matheron, G. (1971). *The Theory of Regionalised variables and its Applications*. Les Cahiers du Centre de Morphologie Mathématique de Fontainebleau 5.
- Matheron, G. (1976). A simple substitute for conditional expectation: the disjunctive kriging. In M. Guarascio, M.

- David, C.J. Huijbregts (Eds.), *Advanced Geostatistics in the Mining Industry* (pp 221"236). Dordrecht: Reidel.
- McKenzie, N. J., Grundy, M. J., Webster, R. and Ringrose-Voase, A. J. (2008). *Guidelines for surveying soil and land resources*. 2nd Ed. (Melbourne: CSIRO PUBLISHING).
- Messina, A., Compagnoni, R., De Vivo, B., Perrone, V., Russo, S., Barbieri, M. and Scott, B. A. (1991). Geological and petrochemical study of the Sila massif plutonic rocks northern Calabria, Italy. *Bollettino della Società Geologica Italiana*, **110**, 1–42.
- Messina, A., Russo, S., Borghi, A., Colonna, V., Compagnoni, R., Caggianelli, A., Fornelli, A. and Piccarreta, G. (1994). Il massiccio della Sila settore settentrionale dell'arco calabro peloritano. *Bollettino della Società Geologica Italiana*, **113**, 539–586.
- Meulenkamp, J. E., Hilgen, F. J. and Voogt, E. (1986). Late Cenozoic sedimentary-tectonic history of the Calabrian Arc/Paleogeography and geodynamics of the Perityrrhenian Area. *Giornale di Geologia*, **48**, 345–359.
- Minato, S. (2002). Simple soil mass balance approach to interpret the distribution of global terrestrial gamma ray dose rates in relation to geology. *Science of the Total Environment*, **298**, 229–231.
- Mohanty, A. K., Sengupta, D., Das, S. K., Saha, S. K. and Van, K. V. (2004). Natural radioactivity and radiation exposure in the high background area at Chhatrapur beach placer deposit of Orissa, India. *Journal of Environmental Radioactivity*, **75**, 15–33.
- Pain C. F., Wilford J. R. and Dohrenwend J. C. (1999). Regolith-landform evolution on Cape York Peninsula. Implications for Mineral Exploration. In: G.Taylor & C. F. Pain (Eds.) *New Approaches to an Old Continent* (pp. 55–66). Perth: CRC LEME.
- Rivoirard, J. (1990). A review of lognormal estimators for in situ reserves. *Mathematical Geology*, **22**, 213–221.
- Roth, C. (1998). Is Lognormal Kriging Suitable for Local Estimation?. *Mathematical Geology*, **30**, 999–1009.
- Sorriso-Valvo, M. and Tansi, C. (1996). Grandi frane e deformazioni gravitative profonde di versante della Calabria-Note illustrative per la carta al 250.000. *Geografia Fisica e Dinamica Quaternaria*, **19**, 395–408.
- Taylor, S. R. (1964). Abundance of chemical elements in the continental crust: a new table. *Geochimica et Cosmochimica Acta*, **28**, 1273–1284.
- Taylor, S. R. (1966). Application of trace element data to problems in petrology. *Physics and Chemistry of the Earth*, **6**, 135–213.
- Tortorici, L. (1982). Lineamenti geologico-strutturali dell'arco calabro-peloritano. *Rendiconti Società Italiana di Mineralogia e Petrologia*, **38**, 927–940.
- Tzortzis, M., Tsertos, H., Christofides, S. and Christodoulides, G. (2003a). Gamma-ray measurements of naturally occurring radioactive samples from Cyprus characteristic geological rocks. *Radiation Measurements*, **37**, 221–229.
- Tzortzis, M., Tsertos, H., Christofides, S. and Christodoulides, G. (2003b). Gamma radiation measurements and dose rates in commercially-used natural tiling rocks (granites). *Journal of Environmental Radioactivity*, **70**, 223–235.
- UNSCEAR, (2000). *Sources and Effects of Ionizing Radiation*. (New York: United Nations).
- Van Dijk, J. P. (1990). Sequence stratigraphy, kinematics and dynamic geohistory of the Crotona Basin (Calabrian Arc, Central Mediterranean): an integrated approach. *Memorie della Società Geologica Italiana*, **44**, 259–285.
- Van Dijk, J. P. (1991). Basin dynamics and sequence stratigraphy in the Calabrian Arc (Central Mediterranean); records and pathways of the Crotona Basin. *Geologie en Mijnbouw*, **70**, 187–201.
- Van Dijk, J. P., Bello, M., Brancaleoni, G. P., Cantarella, G., Costa, V., Frixia, A., Golfetto, F., Merlini, S., Riva, M., Torricelli, S., Toscano, C. and Zerilli, A. (2000). A regional structural model for the northern sector of the Calabrian Arc (southern Italy). *Tectonophysics*, **324**, 267–320.
- Van Dijk, J. P. and Okkes, M. (1991). Neogene tectonostratigraphy and kinematics of Calabrian basins; implications for the geodynamics of the Central Mediterranean. *Tectonophysics*, **196**, 23–60.
- Vassas, C., Pourcelot, L., Vella, C., Carpena, J., Pupin, J. P., Bouisset, P. and Guillot, L. (2006). Mechanisms of enrichment of natural radioactivity along the beaches of the Camargue, France. *Journal of Environmental Radioactivity*, **91**, 146–159.
- Verly, G. (1983). The Multigaussian approach and its application to the estimation of local reserves. *Mathematical Geology*, **15**, 259"286.
- Wackernagel, H. (2003). *Multivariate Geostatistics: an introduction with Applications*. Berlin: Springer-Verlag.
- Weaver, B. L. and Tarney, J. (1984). Empirical approach to estimating the composition of the continental crust. *Nature*, **310**, 575–577.
- Webster, R. and Oliver, M. A. (2007). *Geostatistics for Environmental Scientists*. 2nd Ed. Chichester: Wiley.
- Wildford, J. R., Bierwirth, P. N. and Craig, M. A. (1997). Application of airborne gamma-ray spectrometry in soil/regolith mapping and applied geomorphology. *Journal of Australian Geology & Geophysics*, **17**, 201–216.
- Xinwei, L. and Xiaolan, Z. (2008). <sup>226</sup>Ra, <sup>232</sup>Th and <sup>40</sup>K activities in soils of Cuihua Mountain National Geological Park, China. *Environmental Geology*, **56**, 353–357.
- Zecchin, M., Massari, F., Mellere, D. and Prosser, G. (2004a). Anatomy and evolution of a Mediterranean-type fault bounded basin: the Lower Pliocene of the northern Crotona Basin (Southern Italy). *Basin Research*, **16**, 117–143.
- Zecchin, M., Nalin, R. and Roda, C. (2004b). Raised Pleistocene marine terraces of the Crotona peninsula (Calabria, southern Italy): facies analysis and organization of their deposits. *Sedimentary Geology*, **172**, 165–185.
- Zhitkov, A. S. and Vertman, E. M. (2006). Uranium and Thorium Content of Reference Samples from the Geological Survey of Japan "Igneous Rock Series 1986". *Geostandards and Geoanalytical Research*, **30**, 107–111.